Dislocations in graphene

2008 New J. Phys. 10 053021

(http://iopscience.iop.org/1367-2630/10/5/053021)

New Journal of Physics
The open–access journal for physics

Dislocations in graphene

Ana Carpio[1], Luis L Bonilla[2,3,5], Fernando de Juan[4] and María A H Vozmediano[4]

[1] Departamento de Matemática Aplicada, Universidad Complutense de Madrid, 28040 Madrid, Spain
[2] G Millán Institute for Fluid Dynamics, Nanoscience and Industrial Mathematics, Universidad Carlos III de Madrid, 28911 Leganés, Spain
[3] Unidad Asociada al Instituto de Ciencia de Materiales de Madrid, CSIC, Madrid, Spain
[4] Unidad Asociada ICMM-UC3M, Instituto de Ciencia de Materiales de Madrid, CSIC, Cantoblanco, 28049 Madrid, Spain
E-mail: bonilla@ing.uc3m.es

New Journal of Physics **10** (2008) 053021 (13pp)
Received 15 March 2008
Published 15 May 2008
Online at http://www.njp.org/
doi:10.1088/1367-2630/10/5/053021

Abstract. We study the stability and evolution of various elastic defects in a flat graphene sheet and the electronic properties of the most stable configurations. Two types of dislocations are found to be stable: 'glide' dislocations consisting of heptagon–pentagon pairs, and 'shuffle' dislocations, an octagon with a dangling bond. Unlike the most studied case of carbon nanotubes, Stone Wales defects seem to be dynamically unstable in the planar graphene sheet. Similar defects in which one of the pentagon–heptagon pairs is displaced vertically with respect to the other one are found to be dynamically stable. Shuffle dislocations will give rise to local magnetic moments that can provide an alternative route to magnetism in graphene.

[5] Author to whom any correspondence should be addressed.

Contents

1. Introduction

Graphene has become a very popular material since its recent synthesis [1, 2] and characterization. Among the most interesting properties related to the possible technological applications are its high electron mobility and minimal conductivity at zero bias [3]. Despite the high mobility of most graphene samples, their mean free path of the order of microns [1] implies the presence of defects. Very recent experiments performed on suspended graphene [4, 5] indicate that, besides the influence of the substrate, there must be intrinsic defects in the samples.

The structure of disorder is also crucial to explain the magnetism found in graphite samples [6, 7]. It is now clear that the intrinsic ferromagnetism is linked to defects in the sample altering the coordination of the carbon atoms (vacancies, edges or related defects) [8]. One of the most stable defects found in this work, the shuffle dislocation, has an unpaired electron that can contribute to the magnetic properties of the sample.

Local disorder in graphene has been studied intensely and we refer to the review article [9] for a fairly complete list of references. A different type of disorder is provided by the observation of ripples in suspended graphene [10, 11] and in graphene grown on a substrate [12, 13].

Inspired by the physics of nanotubes and fullerenes, curved graphene has been modeled with curvature induced by topological defects [14]–[18]. In these works, it was shown that conical singularities in the average flat graphene sheet induce characteristic charge anisotropies that could be related to recent observations [19].

The elastic and mechanical properties of graphitic structures have been studied intensely in the past, mostly in the context of understanding the formation of fullerenes and nanotubes. Very little work has been done for the flat graphene sheet [20, 21] and topological defects have often been excluded in these studies. In the fullerene literature, it was established that the formation of topological defects (substitution of a hexagonal ring by other polygons) is the natural way in which the graphitic net heals vacancies and other damage produced for instance by irradiation [22]. Among those, disclinations (isolated pentagon or heptagon rings), dislocations (pentagon–heptagon pairs) and Stone–Wales (SW) defects (special dislocation dipoles) were found to have the least formation energy and activation barriers.

Dislocations and SW defects have been observed in carbon structures [23] and are known to have a strong influence on the electronic properties of nanotubes. The possible role played by nanotube curvature in stabilizing various defects is not yet clear. Glide and shuffle dislocations

in irradiated graphitic structures have been described in [24]. Experimental observations of dislocations have been reported very recently in graphene grown on Ir in [25].

The purposes of this work are to discuss the formation and stability of topological defects (mainly dislocations) in a flat graphene sheet and to analyze the electronic properties of the graphene samples in the presence of the most stable defects. This paper addresses two aspects of physical reality—elasticity and electronics—that are often described using very different language. We intend to reach a general audience and have included brief pedagogical descriptions of the methods used in both disciplines.

This paper is organized as follows: section 2 explains the method used to study the formation and stability of defects and it describes their stable configurations. We find two types of stable dislocations, one with a dangling bond. SW defects are found to be unstable in the flat lattice whereas similar defects in which one of the pentagon–heptagon pairs is displaced vertically with respect to the other one are found to be dynamically stable. Section 3 gives a brief description of the tight binding method and the physical information that can be extracted from it. The electronic characteristics of the two dislocations are derived. In section 4, we present the conclusions and future work.

2. Periodized discrete elasticity and stability of defects

In continuum mechanics, dislocations are usually described by the equations of linear elasticity with singular sources whose supports are the dislocation lines. To describe dislocations in two dimensional (2D) graphene, we should have a more detailed theory which can be used to regularize the corresponding point singularities. It is possible to use *ab initio* theories as regularizers but, provided dislocations are sparse and far from each other, there is a much more economic and insightful alternative. We can discretize appropriately linear elasticity on the hexagonal lattice and then periodize the resulting linear lattice model to allow dislocation gliding. The resulting model equations for the displacement vector $(u'(n,t), v'(n,t))$ (written in primitive coordinates) are [26] (see the appendix for a brief description of their derivation):

$$\frac{\rho a^2}{2}\frac{\partial^2 u'}{\partial t^2} = \frac{\lambda+\mu}{3}[(H-D)u' + (2H+D)v'] + T[(\lambda+3\mu)u' - 2(\lambda+\mu)v'], \quad (1)$$

$$\frac{\rho a^2}{2}\frac{\partial^2 v'}{\partial t^2} = \frac{\lambda+\mu}{3}[(H+2D)u' + (D-H)v'] + T[(\lambda+3\mu)v' - 2(\lambda+\mu)u'], \quad (2)$$

where $n=(x,y)$ is a node A or B on one of the two sublattices in figure 1, ρ is the mass density, a is the lattice constant, and λ and μ are the Lamé coefficients which can be obtained from the elastic constants of (isotropic) graphite in its basal plane, $C_{11} = C_{12} + 2C_{66} = 1060\,\text{GPa}$, $C_{12} = \lambda = 180\,\text{GPa}$ and $C_{66} = \mu = 440\,\text{GPa}$ [27]. Note that $u' = (u - v/\sqrt{3})/a$ and $v' = 2v/(a\sqrt{3})$ are nondimensional because the components of the displacement vector in Cartesian coordinates (u,v) have units of length. The difference operators T, D and H act on functions of the coordinates (x,y) of the node A in figure 1 according to the formulae:

$$Tu' = g(u'(n_1) - u'(A)) + g(u'(n_2) - u'(A)) + g(u'(n_3) - u'(A)), \quad (3)$$

$$Hu' = g(u'(n_6) - u'(A)) + g(u'(n_7) - u'(A)), \quad (4)$$

$$Du' = g(u'(n_4) - u'(A)) + g(u'(n_9) - u'(A)), \quad (5)$$

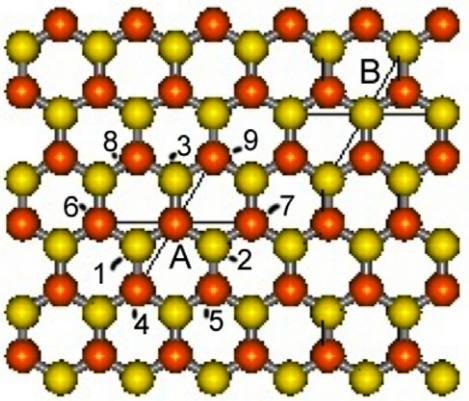

Figure 1. Neighbors of a given atom A. Only the neighbors labeled 1, 2, 3, 4, 6, 7 and 9 are affected by the difference operators T, H and D used in our discrete elasticity model.

where g is a periodic function, with period one, and such that $g(x) \sim x$ as $x \to 0$. Note that the operator T involves finite differences with the three next neighbors of A which belong to sublattice 2, whereas H and D involve differences between atoms belonging to the same sublattice along the primitive directions **a** and **b**, respectively. See figure 1. The same formulae hold if (x, y) is an atom B in the other sublattice. Far from dislocation cores, the finite differences are very small and close to the corresponding differentials. If we Taylor expand these finite difference combinations about (x, y), insert the result in (1) and (2) and write the displacement vector in Cartesian coordinates, we recover the equations of linear elasticity [26]. The role of the periodic function g is to allow dislocation gliding [28]–[30]. When a defect moves, a few atoms change some of their nearest neighbors. We use the periodized difference operators T, D and H in (1) and (2) instead of solving discrete elasticity with an updating algorithm that keeps track of neighbor change. The equations of periodized discrete elasticity (1) and (2) regularize linear elasticity and allow for dislocation motion and for dislocation nucleation [31].

How do we find the defects in graphene that correspond to different edge dislocations? We first substitute (x, y) in the elastic field of a dislocation (such as the edge dislocation of page 57 of [32]) by $x = a\,(x_0' + l + y_0'/2 + m/2)$ and $y = a\sqrt{3}\,(y_0' + m)/2$. l and m are integer numbers that allow the resulting displacement vector to be a vector function of lattice points, which we denote by $\mathbf{U}(l, m)$. The primitive coordinates $x' = x_0' + l$ and $y' = y_0' + m$ are centered on an appropriate point (x_0', y_0') which is different from the origin to avoid the singularity in the elastic field coinciding with a lattice point. We now solve an overdamped periodized discrete elasticity model (in which second-order time derivatives are replaced by first-order ones) with a boundary condition given by **U** and with an initial condition also given by **U**. After a certain relaxation time, the solution of the model evolves to a stable stationary configuration which depends on the location of the origin (x_0', y_0') and on **U**. This stable configuration is also a stable configuration of the original equations of the model (with inertia).

By using the method just sketched, we have obtained that the same dislocation solution of the equations of elasticity may have different cores, which is a familiar fact in crystals with diamond structure and covalent bonds, such as silicon; see page 376 in [33]. The stable configurations corresponding to one edge dislocation are pentagon–heptagon defects

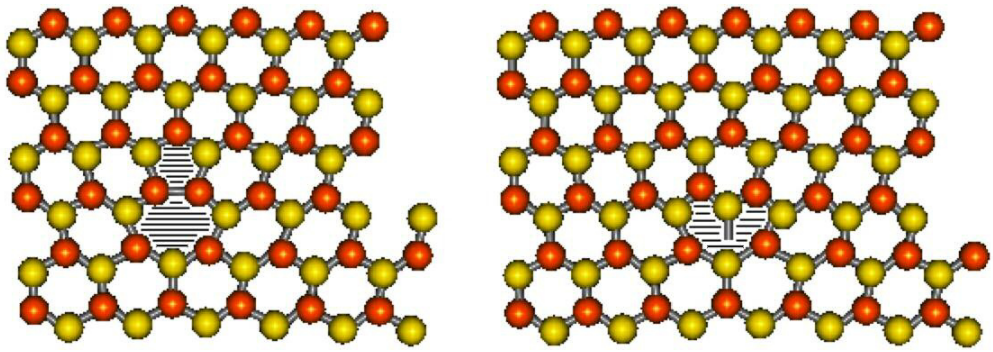

Figure 2. Structure of the glide (left) and shuffle (right) dislocations in the planar graphene lattice.

('glide' dislocations) if the singularity is placed between two atoms that form any non-vertical side of a given hexagon. If the singularity is placed in any other location different from a lattice point, the core of the singularity forms a 'shuffle' dislocation: an octagon having one atom with a dangling bond, as shown in figure 2.

If we use the elastic field of an edge dislocation dipole as initial and boundary conditions, there are again different stable configurations depending on how we place the dislocation cores. An edge dislocation dipole is formed by two edge dislocations with Burgers vectors in opposite directions. Let $\mathbf{E}(x, y)$ be the displacement vector corresponding to the edge dislocation. If $\mathbf{U} = \mathbf{E}(x - x_0, y - y_0 - l/2) - \mathbf{E}(x - x_0, y - y_0)$ ($l = a/\sqrt{3}$ is the hexagon side in terms of the lattice constant a), the stable stationary configuration is that of a vacancy. If $\mathbf{U} = \mathbf{E}(x - x_0, y - y_0 - l) - \mathbf{E}(x - x_0, y - y_0)$, a dynamically stable divacancy (formed by one octagon and two adjacent pentagons) results. An initial configuration corresponding to a SW defect, $\mathbf{E}(x - x_0 - a, y - y_0) - \mathbf{E}(x - x_0, y - y_0)$, is dynamically unstable: at zero applied stress, the two component edge dislocations glide toward each other and annihilate. If a shear stress is applied in the glide direction of the two edge dislocations comprising the SW defect, these defects either continue destroying themselves or, for large enough applied stress, are split in their two component heptagon–pentagon defects that move in opposite directions [26].

Instead of a dislocation dipole, our initial configuration may be a dislocation loop, in which two edge dislocations with opposite Burgers vectors are displaced vertically by one hexagon side: $\mathbf{E}(x - x_0 - a, y - y_0) - \mathbf{E}(x - x_0, y - y_0 - l)$ ($l = a/\sqrt{3}$ is the length of the hexagon side). In principle, the dislocation loop could evolve to an inverse SW defect (7-5-5-7). Instead, this initial configuration evolves toward a single octagon. If we displace the edge dislocations vertically by $l/2$, $\mathbf{E}(x - x_0 - a, y - y_0) - \mathbf{E}(x - x_0, y - y_0 - l/2)$, the resulting dislocation loop evolves toward a single heptagon defect [26].

3. Electronic properties

The electronic structure of the solids and most of their low energy properties are dictated by the position of the Fermi surface, its shape and the amount of electrons available at energies close to it. In the independent electron approximation, valid when the kinetic energy of the electrons is much larger than their mutual interactions, electronics is well described by the band theory. The latter gives two main outputs: geometry of the Fermi surface and density of states (DOS) at the Fermi level [34].

The tight-binding approximation assumes that the electrons in the crystal behave much like an assembly of constituent atoms. It works by replacing the many-body Hamiltonian operator by a matrix Hamiltonian. The solution to the time-independent single electron Schrödinger equation is well approximated by a linear combination of atomic orbitals. These form a minimal set of short range basis functions ϕ_i—that we do not need to specify—and the full wavefunction at site i is given by

$$\Psi_i = \sum_{ij} C_{ij}\phi_j.$$

The electron density at a lattice site pq can be computed as

$$P_{pq} = 2\sum_{k}^{occ}\sum_{pq} C_{pk}C_{qk}^{*}.$$

The tight binding energy is given by

$$E = \sum_{pq} P_{pq}h_{pq} = 2\sum_{k}^{occ}\sum_{pq} C_{pk}C_{qk}^{*}h_{pq},$$

where hpq is the element of the matrix Hamiltonian.

The advantage of the method is that matrix elements

$$h_{pq} = \langle p|H|q\rangle = \int \mathrm{d}\mathbf{r}\phi_p^{*}(\mathbf{r})H\phi_q(\mathbf{r}),$$

$$S_{pq} = \langle \phi_p|\phi_q\rangle = \int \mathrm{d}\mathbf{r}\phi_p^{*}(\mathbf{r})\phi_q(\mathbf{r}),$$

are not explicitly calculated but approximated by phenomenological parameters that depend on the geometry of the lattice and the nature of the orbitals. The full strength of the tight binding approximation is related to the perfect-discrete-translational invariance of the periodic lattice. The use of Bloch wavefunctions in Fourier space allows a full description of the dispersion relation with the only input of the overlapping integrals that can be indirectly deduced from experiments. Since we are going to treat lattice defects that break translational invariance we will stay in real space and adopt the simplest possible approximation: site energies are set to zero and overlapping integrals are nonzero only for nearest neighbor atoms. The hopping integral in graphene is estimated to be of the order of $t \sim 2.7$ eV. In summary, and in a very general sense, the electronic structure within the tight binding approximation is obtained simply by defining a lattice with links, and diagonalizing the Hamiltonian, a matrix with elements h_{ij} equal to t, if atom i is linked to j and zero otherwise. This is the calculation that we have performed. The honeycomb lattice is generated by moving the unit cell made of two atoms along the two unit vectors that generate the lattice as described in [34].

A full analysis of the tight binding structure of graphene can be seen in the original paper [35] and in the reference book [36]. Its main outcome is that the Fermi surface reduces to two points and the DOS vanishes at the Fermi energy which, in turn, determines the semimetallic character of the material. The DOS is very important to characterize the electronic and transport properties of the samples. Disorder can open a gap or, more often, induce a finite DOS. Real samples have localized states at (or around) zero energy which are induced close to edges,

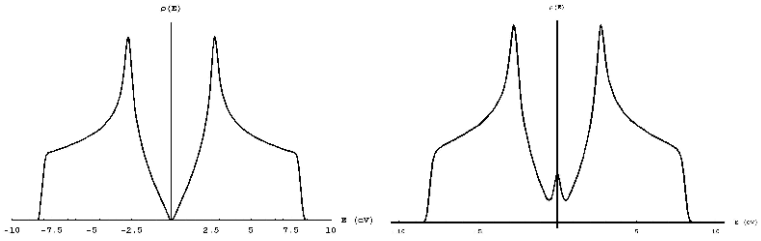

Figure 3. Total DOS. Left panel: clean graphene. Right panel: graphene ribbon with zigzag edges.

vacancies, ad-atoms or other defects. These midgap states can form very narrow bands, where the electronic interactions become important and may lead to electronic instabilities, particularly ferromagnetism [37].

The DOS of an ideal graphene sheet is shown in the left panel of figure 3. It vanishes at the Fermi energy what determines the semi-metallic character of the material. Defects in the lattice very often induce states at zero energy. An important class is that of edge states induced by certain boundaries in finite lattices or real samples (graphene nanoribbons). Zigzag (armchair) edges can be seen in the horizontal (vertical) borders in figure 1. Zigzag edges with uncoordinated atoms belonging to the same sublattice induce a number of zero energy edge states proportional to the amount of unpaired lattice sites [38]. They are important in potential applications. These energy states are localized at the edges as can be seen in the local DOS (LDOS) of figure 4. When studying electronic properties via numerical simulations, it is important to disentangle the low-energy effects coming from the boundary from those which are intrinsic to the defects under study. The DOS of a graphene nanoribbon with zigzag edges is shown for comparison in the right panel of figure 3.

3.1. Electronic structure of single dislocations

As discussed in section 2, the 'glide' and 'shuffle' dislocations shown in figure 2 are stable in the graphene sheet. We have performed a tight binding calculation for these two types of dislocations. Figure 4 shows the configuration of the lattice for the dislocations depicted in the inset where the atoms that constitute the defect are numbered. The extra rows of atoms characteristic of these edge dislocations are shown in red. The area of the circles is proportional to the squared wavefunction for one of the lowest energy eigenvalues. The extra charge appearing at the shuffle dislocation is due to the dangling bond attached to it. Figure 4 also shows the extra charge at the zigzag edges.

In figure 5, we show the LDOS for the five sites around the defect numbered in the inset of figure 4 and for an extra site located at a certain distance from the defect. The LDOS is drastically distorted at the defects but rapidly recovers the normal shape away from the center of the defect. The pentagon–heptagon pair (glide dislocation) breaks the electron–hole symmetry of the lattice but the corresponding LDOS resembles that of the perfect lattice shown in figure 3. The LDOS at zero energy is not zero, but it has a minimum in all the cases. The sixth graph shows the LDOS at an atom located six lattice units apart from the defect. This is the distance at which the influence of the dislocation ceases to be noticeable.

The shuffle dislocation has a more pronounced effect on the LDOS. As can be seen in figure 5, at zero energy there appear sharp peaks at the position of the dangling bond atom

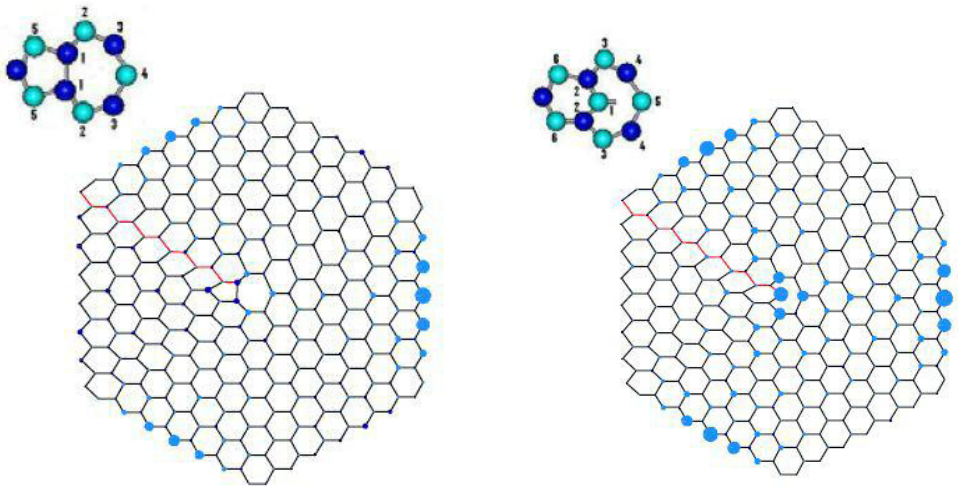

Figure 4. Left: lattice structure and charge density for a low energy eigenstate in the presence of a glide dislocation shown in the inset. Right: same for the shuffle dislocation.

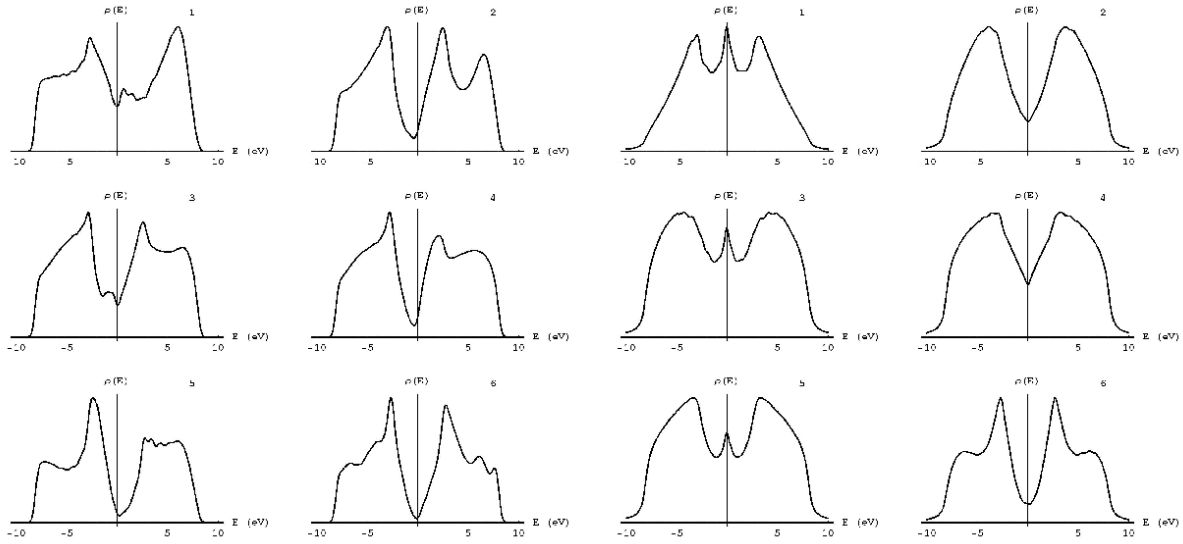

Figure 5. Left: for the graphene sample with a glide dislocation depicted in figure 4, LDOS at the numbered sites around the defect shown in the inset of figure 4. Right: same for the sample with a shuffle dislocation.

and at neighboring sites of the same sublattice whereas dips in the LDOS appear at the sites of the opposite sublattice. The distortion in the LDOS decays faster with distance in the case of a shuffle dislocation than in the case of a heptagon–pentagon pair. The right panel of figure 5 shows that the DOS of the perfect lattice is already recovered at position 6 of the inset in figure 4, one lattice distance away from the defect. The mid gap state induced by the defect is strongly peaked at the defect position, similarly to what happens with the zigzag edges states. This type of dislocation does not break the electron–hole symmetry of the lattice.

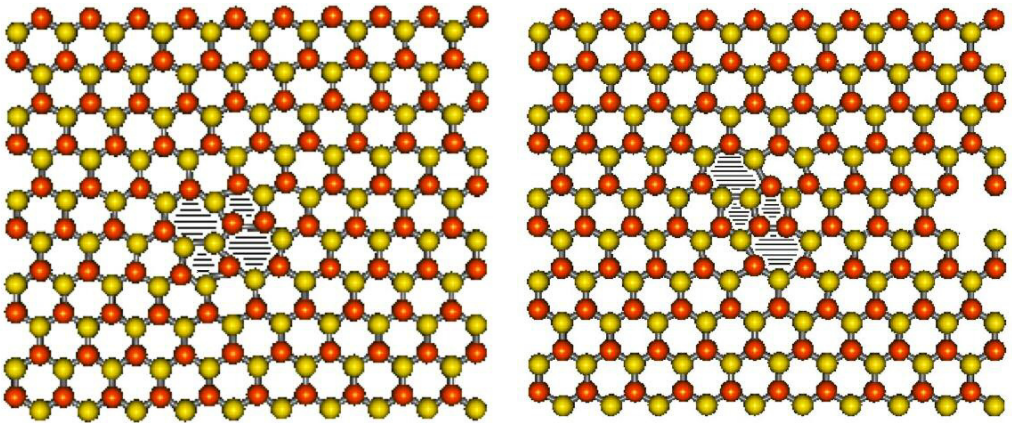

Figure 6. Left: lattice structure of a SW defect. Right: same for the dislocation dipole described in the text.

3.2. Defects of SW type

One of the best studied defects in the carbon nanotube literature is the SW defect [39]. It consists of two pentagon–heptagon pairs that can be obtained by a 90° rotation of a lattice bond. The resulting structure is shown in the left-hand side of figure 6. These defects play a very important role in the surface reconstruction of irradiated nanotubes [40] and affect their mechanical properties. From the standpoint of elasticity, they can be seen as two identical edge dislocations that have opposite Burgers vectors and share the same glide line. They appear to be dynamically unstable: their component edge dislocations glide towards each other and annihilate, leaving the undistorted lattice as the final configuration [26]. Our results have been obtained by numerically solving the equations of the model with an initial condition corresponding to a SW defect. Since this initial condition evolves towards the undistorted lattice, we may conclude that either the SW defect is dynamically unstable or that it is stable with such a small basin of attraction that, unless the initial condition happens to be inside this basin, any numerical errors move the system away from it.

A type of defect whose final configuration is very similar—two heptagon–pentagon pairs—is shown in the right panel of figure 6. It is a dislocation dipole whose two edge dislocations with opposite Burgers vectors are displaced vertically by one lattice unit. By solving the periodized discrete elasticity model of section 2, we can show that this configuration is dynamically stable. The electronic structure of these two defects is depicted in figures 7 and 8. These dipole defects induce a stronger local distortion of the charge density than single dislocations. While the real SW defect does not alter the structure of the lattice edges, the other dislocation dipole has two extra atoms as compared to the perfect lattice, and therefore it alters the structure of its edges. This is clearly visible in figure 6. The presence of these defects can affect the electronic properties of real samples.

4. Conclusions and discussion

We have used a regularization of continuum elasticity on the honeycomb lattice to explore the stability and evolution of topological defects. Two types of dislocations are stable: pentagon–heptagon pairs (‘glide’ dislocations) and ‘shuffle’ dislocations: an octagon having one atom with a dangling bond. They are shown in figure 2.

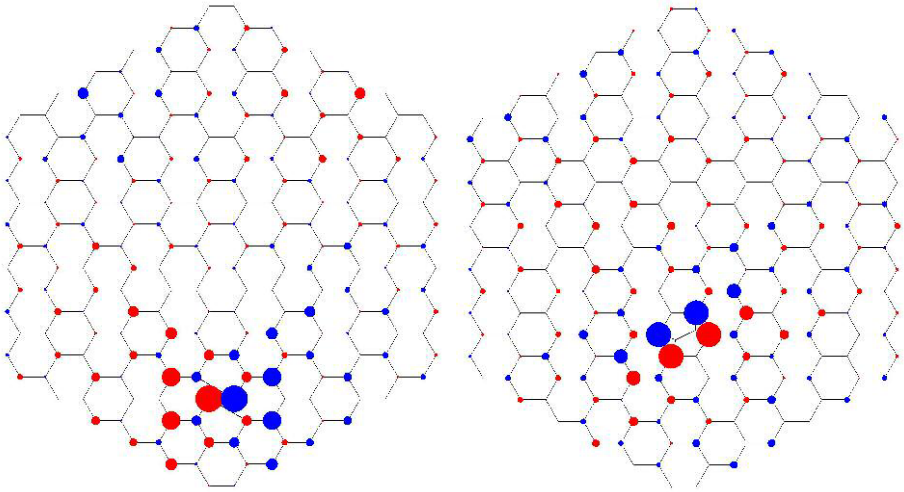

Figure 7. Left: lattice structure and charge density for the fourth positive-energy eigenstate in the presence of a SW defect. Right: same for the dislocation dipole described in the text.

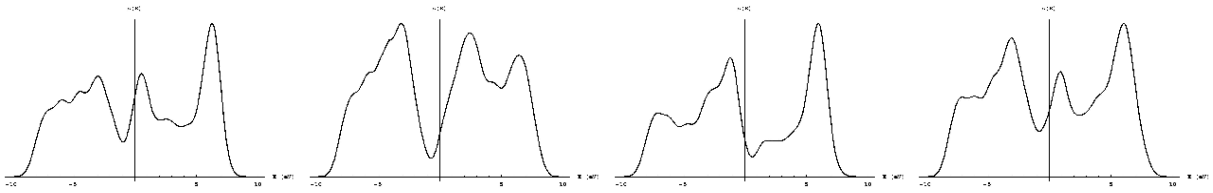

Figure 8. From left to right: LDOS of a real SW defect at the site shared by the two adjacent pentagons and at its nearest neighbor. LDOS of the dislocation dipole discussed in the text at the site shared by the two heptagons and at its nearest neighbor.

Both defects induce distortions in the LDOS at low energies that decay rapidly with the distance to the defect. The presence of a dangling bond in the shuffle dislocations drastically enhances these effects but, as in the case of zigzag states, the low energy states are very localized. Dislocations in metals have been proposed to give rise to electron localization in 3D systems [41, 42] although the tendency to localization seems to be much weaker in 2D crystals [43]. The nature of the lowest energy states found in this work indicates that dislocations will not localize states at zero energy in the honeycomb lattice in agreement with [43], but we will perform a more systematic analysis of this issue in the future.

The main physical effect of the shuffle dislocations will be related to the nucleation of magnetic moments at the dangling bonds. Work in this direction is in progress.

Regarding configurations of edge dislocation dipoles in discrete elasticity, vacancies and di-vacancies are stable but SW defects are very likely to be dynamically unstable. This situation is to be confronted with what happens in the carbon nanotubes where SW defects are stable. This points to the idea that curvature and geometry play a role in their stabilization. We are also working in this direction.

A defect similar to the SW consists of a dislocation dipole whose component dislocations are displaced one lattice unit. This defect is dynamically stable and can give rise to a large

local distortion of the electronic density. The defects discussed in this work are very likely to be present in real samples of both graphene and nanoribbons. They will affect the transport properties of the samples and they will also alter the configuration of the sample edges. This must be taken into consideration in the cases when perfect tailoring of the edges is important.

Acknowledgments

This research was supported by the Spanish MECD grants MAT2005-05730-C02-01, MAT2005-05730-C02-02, FIS2005-05478-C02-01 and by the Autonomous Region of Madrid under grants S-0505/ENE/0229 (COMLIMAMS) and CM-910143 and by PR27/05-13939. The *Ferrocarbon* project from the European Union under Contract 12881 (NEST) is also acknowledged.

Appendix. Derivation of the discrete model equations [26]

The Navier equations of linear isotropic elasticity for a 2D hexagonal lattice are [26]:

$$\rho\frac{\partial^2 u}{\partial t^2} = C_{11}\frac{\partial^2 u}{\partial x^2} + C_{66}\frac{\partial^2 u}{\partial y^2} + (C_{66}+C_{12})\frac{\partial^2 v}{\partial x\,\partial y}, \tag{A.1}$$

$$\rho\frac{\partial^2 v}{\partial t^2} = C_{66}\frac{\partial^2 v}{\partial x^2} + C_{11}\frac{\partial^2 v}{\partial y^2} + (C_{66}+C_{12})\frac{\partial^2 u}{\partial x\,\partial y}, \tag{A.2}$$

where (u, v) is the displacement vector, ρ is the mass density and $C_{66} = \mu$, $C_{12} = \lambda$ and $C_{11} = \lambda + 2\mu$ are the elastic constants in the basal plane of graphite. λ and μ are the Lamé coefficients of isotropic elasticity.

We want to regularize the Navier equations in a hexagonal lattice so that the solutions of the resulting discrete model are not singular at the core of a dislocation and that dislocation glide motion is allowed along primitive directions. To do so, we shall discretize conveniently the Navier equations and then put back the translation symmetry of the lattice by introducing appropriate periodic functions.

To discretize the Navier equations, we denote by (x, y) the coordinates of the atom A in figure 1. Besides the nearest neighbors with coordinates $n_1 = (x - a/2, y - a/(2\sqrt{3}))$, $n_2 = (x + a/2, y - a/(2\sqrt{3}))$ and $n_3 = (x, y + a/2)$, there are four atoms separated from A by the primitive vectors $(\pm a, 0)$, $\pm(a/2, a\sqrt{3}/2)$, namely $n_6 = (x - a, y)$, $n_7 = (x + a, y)$, $n_4 = (x - a/2, y - a\sqrt{3}/2)$ and $n_9 = (x + a/2, y + a\sqrt{3}/2)$. With the finite differences between A, its three nearest neighbors and its four next nearest neighbors along primitive directions, we may form the following combinations

$$T_l u = [u(n_1) - u(A)] + [u(n_2) - u(A)] + [u(n_3) - u(A)], \tag{A.3}$$

$$H_l u = [u(n_6) - u(A)] + [u(n_7) - u(A)], \tag{A.4}$$

$$D_l u = [u(n_4) - u(A)] + [u(n_9) - u(A)]. \tag{A.5}$$

Taylor expansions of these finite difference combinations about (x, y) yield

$$T_l u \sim \left(\frac{\partial^2 u}{\partial x^2} + \frac{\partial^2 u}{\partial y^2}\right)\frac{a^2}{4},$$

$$H_l u \sim \frac{\partial^2 u}{\partial x^2}\, a^2,$$
$$D_l u \sim \left(\frac{1}{4}\frac{\partial^2 u}{\partial x^2} + \frac{\sqrt{3}}{4}\frac{\partial^2 u}{\partial x \partial y} + \frac{3}{4}\frac{\partial^2 u}{\partial y^2}\right) a^2,$$

as $a \to 0$. In equations (A.1) and (A.2), we now substitute $H_l u/a^2$, $(4T_l - H_l)u/a^2$ and $2(D_l - 3T_l + H_l/2)u/(\sqrt{3}a^2)$ for $\partial^2 u/\partial x^2$, $\partial^2 u/\partial y^2$ and $\partial^2 u/\partial x \partial y$, respectively, with similar substitutions for the derivatives of v. In terms of the Lamé coefficients, the following equations are then obtained:

$$\rho a^2 \frac{\partial^2 u}{\partial t^2} = 4\mu\, T_l u + (\lambda + \mu)\, H_l u + \frac{2(\mu+\lambda)}{\sqrt{3}}\left(D_l - 3T_l + \frac{1}{2}H_l\right) v, \tag{A.6}$$

$$\rho a^2 \frac{\partial^2 v}{\partial t^2} = 4\mu\, T_l v + (\lambda + \mu)\, (4T_l - H_l) v + \frac{2(\mu+\lambda)}{\sqrt{3}}\left(D_l - 3T_l + \frac{1}{2}H_l\right) u, \tag{A.7}$$

at every point of the lattice. By construction, these equations become the Navier equations (A.1) and (A.2) in the limit as $a \to 0$. They can be written in primitive coordinates as (1) and (2) (with operators T_l, H_l and D_l instead of T, H and D, respectively) by using the transformation $u' = (u - v/\sqrt{3})/a$ and $v' = 2v/(a\sqrt{3})$. The resulting model is linear and does not allow for the changes of neighbors involved in defect motion. An obvious way to achieve this is to update the neighbors as a defect moves. Models such as (1)–(2) (with operators T_l, H_l and D_l) would have the same appearance, but the neighbors n_i would keep their relative positions only at the start. At each time step, we could keep track of the position of the different atoms and update the coordinates of the n_i. Updating neighbors is convenient but it has a high computational cost and analytical studies of the resulting models are not easy. In simple geometries, we can avoid updating by introducing a periodic function of differences in the primitive directions that automatically describes link breakup and union associated with defect motion. Besides reducing computational cost, the resulting periodized discrete elasticity models allow analytical studies of defect deppining [28]–[30], motion and nucleation [31].

To restore crystal periodicity, we replace the linear operators T_l, H_l and D_l of (A.3), (A.4) and (A.5) in equations (A.6) and (A.7) by their periodic versions (3), (4) and (5), thereby obtaining equations (1) and (2) in primitive coordinates. About four atomic spacings away from the core of a dislocation, the solution of the discrete model is very close to the known solution of linear elasticity, so that a lattice with 8×8 lattice spacings is sufficient to numerically calculate dislocation cores. Figures 2 and 6 have been calculated using a lattice with 18×18 lattice spacings ($36^2 = 1296$ atoms).

Selected results of [26] are described in section 2.

References

[1] Novoselov K S, Geim A K, Morozov S V, Jiang D, Katsnelson M I, Grigorieva I V, Dubonos S V and Firsov A A 2005 *Nature* **438** 197
[2] Zhang Y B, Tan Y-W, Stormer H L and Kim P 2005 *Nature* **438** 201
[3] Geim A K and Novoselov K S 2007 *Nat. Mater.* **6** 183
[4] Bolotin K I, Sikes K J, Jiang Z, Fudenberg G, Hone J, Kim P and Stormer H L 2008 *Preprint* 0802.2389
[5] Du X, Skachko I, Barker A and Andrei E Y 2008 *Preprint* 0802.2933

[6] Ohldag H, Tyliszczak T, Hohne R, Spemann D, Esquinazi P, Ungureanu M and Butz T 2007 *Phys. Rev. Lett.* **98** 187204
[7] Barzola-Quiquia J, Esquinazi P, Rothermel M, Spemann D, Butz T and García N 2007 *Phys. Rev.* B **76** 161403
[8] Kusakabe K and Maruyama M 2003 *Phys. Rev.* B **67** 092406
[9] Neto A H C, Guinea F, Peres N M R, Novoselov K S and Geim A K 2008 *Rev. Mod. Phys.* at press (*Preprint* 0709.1163)
[10] Meyer J C, Geim A K, Katsnelson M I, Novoselov K S, Booth T J and Roth S 2007 *Nature* **446** 60
[11] Meyer J C, Geim A K, Katsnelson M I, Novoselov K S, Obergfell D, Roth S, Girit C and Zettl A 2007 *Solid State Commun.* **143** 101
[12] Stolyarova E, Rim K T, Ryu S, Maultzsch J, Kim P, Brus L E, Heinz T F, Hybertsen M S and Flynn G W 2007 *Proc. Natl Acad. Sci. USA* **104** 9209
[13] Ishigami M, Chen J H, Cullen W G, Fuhrer M S and Williams E D 2007 *Nano Lett.* **7** 1643
[14] Tamura R and Tsukada M 1994 *Phys. Rev.* B **49** 7697
[15] Charlier J C and Rignanese G M 2001 *Phys. Rev. Lett.* **86** 5970
[16] González J, Guinea F and Vozmediano M A H 2001 *Phys. Rev.* B **63** 134421
[17] Cortijo A and Vozmediano M A H 2007 *Europhys. Lett.* **77** 47002
[18] Cortijo A and Vozmediano M A H 2007 *Nucl. Phys.* B **763** 293
[19] Martin J, Akerman N, Ulbricht G, Lohmann T, Smet J H, von Klitzing K and Yacoby A 2008 *Nat. Phys.* **4** 144
[20] Fasolino A, Los J H and Katsnelson M I 2007 *Nat. Mater.* **6** 858
[21] Castro-Neto A and Kim E 2007 *Preprint* cond-mat/0702562
[22] Lee G-D, Wang C Z, Yoon E, Hwang N-M, Kim D-Y and Ho K M 2005 *Phys. Rev. Lett.* **95** 205501
[23] Hashimoto A, Suenaġa K, Gloter A, Urita K and Ijima S 2004 *Nature* **430** 870
[24] Ewels C P, Heggie M I and Briddon P R 2002 *Chem. Phys. Lett.* **351** 178
[25] Coraux J, N'Diaye A T, Busse C and Michely T 2008 *Nano Lett.* **8** 565
[26] Carpio A and Bonilla L L 2008 submitted
[27] Blakeslee O L, Proctor D G, Seldin E J, Spence G B and Weng T 1970 *J. Appl. Phys.* **41** 3373
[28] Carpio A and Bonilla L L 2003 *Phys. Rev. Lett.* **90** 135502
[29] Carpio A and Bonilla L L 2005 *Phys. Rev.* B **71** 134105
[30] Carpio A, Bonilla L L and Plans I 2007 *Physica* A **376** 361
[31] Plans I, Carpio A and Bonilla L L 2008 *Europhys. Lett.* **81** 36001
[32] Nabarro F R N 1967 *Theory of Crystal Dislocations* (Oxford: Oxford University Press)
[33] Hirth J P and Lothe J 1982 *Theory of Dislocations* 2nd edn (New York: Wiley)
[34] Kittel C 1996 *Introduction to Solid State Physics* 7th edn (New York: Wiley)
[35] Wallace P R 1947 *Phys. Rev.* **71** 622
[36] Saito R, Dresselhaus G and Dresselhaus M S 1998 *Physical Properties of Carbon Nanotubes* (Singapore: World Scientific)
[37] Guinea F, Katsnelson M I and Vozmediano M A H 2008 *Phys. Rev.* B **77** 075422
[38] Fujita M, Wakabayashi K, Nakada K and Kusakabe K 1996 *J. Phys. Soc. Japan* **65** 1920
[39] Slonczewski J C and Weiss P R 1958 *Phys. Rev.* **109** 272
[40] Ajayan P M, Ravikumar V and Charlier J-C 1998 *Phys. Rev. Lett.* **81** 1437
[41] Kontsevoi O Yu, Mryasov O N, Gornostyrev Yu N, Freeman A J, Katsnelson M I and Trefilov A V 1998 *Phil. Mag. Lett.* **78** 427
[42] Kontsevoi O Yu, Gornostyrev Yu N, Mryasov O N, Freeman A J, Katsnelson M I and Trefilov A V 2001 *Phys. Rev.* B **64** 134103
[43] Anokhin A O, Gal'perin M I, Gornostyrev Yu N, Katsnelson M I and Trefilov A V 1994 *JETP Lett.* **59** 369